THE EFFECT OF SOOT MODELING ON THERMAL RADIATION IN BUOYANT TURBULENT DIFFUSION FLAMES

A Snegirev[1, 3], **E. Kokovina**[1], **A. Tsoy**[1], **J. Harris**[2], **T. Wu**[2]
[1] Peter the Great St-Petersburg Polytechnic University, St-Petersburg, 195251 Russia
[2] The Boeing Company, Seattle, WA 98124 USA

E-mail: a.snegirev@phmf.spbstu.ru

Abstract. Radiative impact of buoyant turbulent diffusion flames is the driving force in fire development. Radiation emission and re-absorption is controlled by gaseous combustion products, mainly CO_2 and H_2O, and by soot. Relative contribution of gas and soot radiation depends on the fuel sooting propensity and on soot distribution in the flame. Soot modeling approaches incorporated in big commercial codes were developed and calibrated for momentum-dominated jet flames, and these approaches must be re-evaluated when applied to the buoyant flames occurring in fires. The purpose of this work is to evaluate the effect of the soot models available in ANSYS FLUENT on the predictions of the radiative fluxes produced by the buoyant turbulent diffusion flames with considerably different soot yields. By means of large eddy simulations, we assess capability of the Moss-Brooks soot formation model combined with two soot oxidation submodels to predict methane- and heptane-fuelled fires, for which radiative flux measurements are available in the literature. We demonstrate that the soot oxidation models could be equally important as soot formation ones to predict the soot yield in the overfire region. Contribution of soot in the radiation emission by the flame is also examined, and predicted radiative fluxes are compared to published experimental data.

1. Introduction

Natural fires are mainly driven by turbulent diffusion combustion in buoyancy dominated flames. The effect of buoyancy, wide range of stoichiometry covering very lean (over-ventilated) and very reach (under-ventilated) flames, large amount of soot and importance of soot radiation makes combustion in natural fires to be rather distinct from that in jet flames occurring in engines and turbines. There are growing experimental evidences that buoyancy-dominated flames exhibit markedly higher peak soot volume fractions occurring lower relative to the flame length, in contrast with the momentum-dominated flames [1]. It implies that conclusions on model validity derived for conditions of engines and turbines may not be transferrable to fire conditions.

A series of validation studies is currently undertaken by the authors to apply ANSYS FLUENT 14.5 for fire related problems of increasing complexity. Based on the large eddy simulation results for 176 kW methane fire by Hostikka et al. [2] and 116 kW heptane fire by Klassen and Gore [3], this paper highlights the effect of soot modeling. This is done by applying and comparing three soot models composed of soot formation and oxidation submodels (the one-step model by Khan and

[3] To whom any correspondence should be addressed.

Greeves, the two-step model by Tesner et al., and the Moss-Brookes model), available in the software. In this work we focus on the Moss-Brooks soot formation model and show that the soot oxidation models are equally important to predict the soot yield in the overfire region. We also examine contribution of soot in the radiation emission by the flame and compare predicted radiative fluxes to those measured in [2] and [3].

2. The experimental scenarios and computational setup

The experiments with low-soot methane flame were performed by Hostikka et al. [2] in a quiescent air above the water-cooled 0.38 m diameter burner. Here we consider Case D, with the fuel flow rate of 3.516 g/s corresponding to the heat release rate of 175.8 kW. Computational domain is the vertical cylinder of 1.62 m diameter and 2.28 m height, with the burner surface symmetrically located in flash with the floor level. Non-structured mesh in the horizontal plane is projected in vertical direction throughout the computational domain. Height of the domain was spanned by 186 layers thereby providing uniform vertical cell size of 12.26 mm. Maximum horizontal cell size in the flame zone was also selected to be close to this value. Total amount of grid cells is 764 646.

A strongly sooting flame is represented by the experimental prototype studied by Klassen and Gore in [3]. Similar to the previous case, circular 0.3 m diameter burner is located coaxially with the cylindrical computational domain (1.65 m diameter, 3 m height), although elevated 15 cm above the floor level (figure 1). Heptane fuel is supplied at a rate of 2.56 g/s, which corresponds to the heat release rate of 116 kW. The burner diameter was spanned by 32 grid cells thereby providing the cell size of 9.375 mm in the region above the burner. The mesh with 320 vertical layers included 1 146 224 cells.

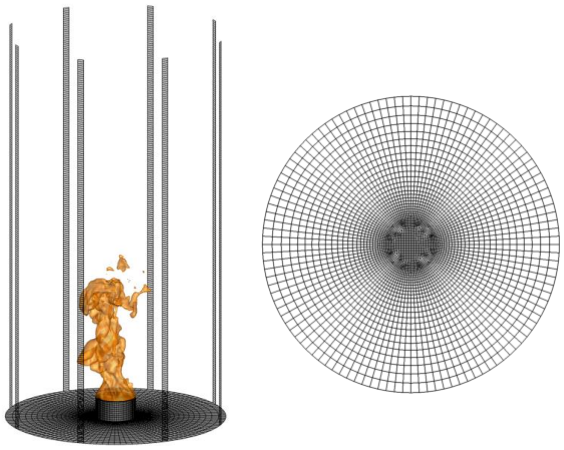

Figure 1. Computational mesh (heptane flame).

In both cases the meshes were constructed to allow for the solid vertical strips replicating locations of radiometers used in the experiments (0.732 m and 0.825 m away from the flame axis in the methane flame and heptane flames, respectively). As shown in figure 1, eight identical strips are used to keep axial symmetry of the flow and to average the predicted heat fluxes from the pulsating flame. Solid strips are required to use WALL boundary condition which is necessary in FLUENT to get information on the surface incident radiation.

Discretizations of highest available order were activated both in space (bounded central differences for momentum, second order upwind for energy and species equations) and time (bounded second order implicit formulation). Fixed time step of 1 ms provided maximum Courant number close to one.

Discretization accuracy and mesh resolution are expected to be sufficient to resolve most of the turbulent kinetic energy, which was checked by analyzing the power spectrum of velocity fluctuations. However, the internal structure of reaction zones cannot be resolved, and it results in underestimated instantaneous flamelet temperatures and mean radiative emission. Nevertheless, as shown below, the simulation results closely resemble time-averaged measurement data.

3. Model description

3.1. Flow, turbulence and combustion

The large eddy simulation (LES) approach was applied for turbulence with the static subgrid Smagorinsky-Lilly model. We used FLUENT default settings of $C_S = 0.1$, energy Prandtl number 0.85 and Schmidt number 0.7. The eddy dissipation model is used in this work for gas combustion. This approach assumes a single-step infinitely fast irreversible global reaction and evaluates fuel burning rate as inversely proportional to the subgrid mixing time scale. The latter is set to be inversely proportional to the second invariant of the resolved strain rate. This approach does not take into account the finite rate chemistry, and considering ignition or extinction would require an additional subgrid model such as that developed in [4, 5].

3.2. Thermal radiation

The discrete ordinates radiation model (DOM) is used to solve the radiative transfer equation for radiation intensities. To weaken the ray effect, we triplicated the default values for angular discretization and performed the simulations with $N_\theta = N_\phi = 6$ control angles and $n_\theta = n_\phi = 3$ sub-angles, using three energy iterations per one radiation iteration. Since we used six iterations for flow equations per time step, the DOM was applied twice at each time step.

The weighted-sum-of-gray-gases model (WSGGM) was used to approximately allow for the spectral properties of the gaseous (CO_2 and H_2O) combustion products and soot [7], [8]. The mean path length of 0.24 m was evaluated assuming cylindrical flame shape with the diameter equal to that of the burner and the height estimated using the empirical relation by Heskestad [6].

The soot absorption coefficient is evaluated as an approximation to data from [7] and [8], $\kappa_{soot} = \rho Y_{soot}\left(c_1 + c_2\left(T - T_*\right)\right)$, where ρ and Y_{soot} are the mixture density and the soot mass fraction, $c_1 =$ 1232.4 m^2/kg, $c_2 = 0.59155$ m^2/(kg·K), and $T_* = 2000$ K. Soot contribution in the gas-soot mixture is accounted via the soot absorption coefficient, κ_{soot}, added to that of gas to obtain the effective absorption coefficient, $\kappa = \kappa_{gas} + \kappa_{soot}$.

Radiation emission term in the radiative transfer equation is modelled as $\tilde{\kappa}\sigma\tilde{T}^4/\pi$, where $\tilde{T}$ and $\tilde{\kappa}$ are the instantaneous resolved quantities. No subgrid modeling of turbulence-radiation interaction (TRI) has been undertaken, which can only be tolerated if mesh resolution is sufficiently high. Provided the error introduced by the inequality, $\kappa T^4 \neq \tilde{\kappa}\tilde{T}^4$, is small enough, this is a more fundamental approach than that used in practical fire simulations, in which the local emission term is recalibrated to provide the total radiated energy to be equal to a pre-assumed fraction, f_r, of the total heat release rate in the flame.

3.3. Soot modeling

In the Moss-Brookes model, which was introduced in a series of works including [9], two transport equations for soot mass fraction and normalized particle concentration are solved:

$$\frac{\partial \rho Y_{soot}}{\partial t} + \nabla \rho Y_{soot}\mathbf{V} = \nabla \frac{\mu_T}{\sigma_{soot}} \nabla Y_{soot} + \dot{R}_{soot}, \tag{1}$$

$$\frac{\partial \rho n^*}{\partial t} + \nabla \rho n^* \vec{\mathbf{V}} = \nabla \frac{\mu_T}{\sigma_{soot}} \nabla n^* + \dot{n}^*. \tag{2}$$

In equation (2), $n^* = N^*/\rho = \left(N/\rho\right)/10^{15}$ is the normalized nuclei concentration, and the particle source term is

$$\dot{n}^* = \frac{1}{10^{15}}\left(\underbrace{C_\alpha N_A \left(\frac{X_{prec} P}{\mathscr{R} T}\right)^l \exp\left(-\frac{T_\alpha}{T}\right)}_{Spontaneous\ nucleation} - \underbrace{C_\beta \left(\frac{24 \mathscr{R} T}{\rho_{soot} N_A}\right)^{1/2} d_p^{1/2} N^2}_{Free-molecular\ coagulation} \right), \tag{3}$$

where $N = 10^{15} N^* = 10^{15} \rho n^*$ (particle/m^3) is the particle concentration, C_α, C_β, and l are the model constants, N_A = 6.022·10^{26} kmol^{-1} is the Avogadro number, X_{prec} is the mole fraction of soot precursor, d_p is the mean particle diameter.

The source term for the soot mass fraction in equation (1) accounts for spontaneous nucleation, surface particle growth, and oxidation by hydroxyl radical and molecular oxygen:

$$\dot{R}_{soot} = \underbrace{M_{p,0} C_\alpha \left(\frac{X_{prec} P}{\mathscr{R} T}\right)^l \exp\left(-\frac{T_\alpha}{T}\right)}_{Nucleation} + \underbrace{C_\gamma \left(\frac{X_{prec} P}{\mathscr{R} T}\right)^m \exp\left(-\frac{T_\gamma}{T}\right)\left((\pi N)^{1/3}\left(6\frac{\rho Y_{soot}}{\rho_{soot}}\right)^{2/3}\right)^n}_{Surface\ growth} - \tag{4}$$

$$- C_{ox}\left(\underbrace{C_{\omega,1}\eta_{coll}\left(\frac{X_{OH} P}{\mathscr{R} T}\right)}_{Fenimore\text{-}Jones\ oxidation} + \underbrace{C_{\omega,2}\left(\frac{X_{O_2} P}{\mathscr{R} T}\right)\exp\left(-\frac{T_{\omega,2}}{T}\right)}_{Lee\ oxidation} \right) \sqrt{T}\,(\pi N)^{1/3}\left(6\frac{\rho Y_{soot}}{\rho_{soot}}\right)^{2/3}$$

where $M_{p,0}$ is the mass of an incipient soot particle, X_{OH} is the hydroxyl radical mole fraction, which is assumed to be the dominant oxidizing agent in the Fenimore-Jones model, X_{O_2} is the molecular oxygen mole fraction, $T_{\omega,2}$ is the activation temperature for oxidation by O_2. The default options of partial equilibrium for [OH] and equilibrium for [O] where retained. The full set of numerical values for the model constants is reported in ANSYS FLUENT Theory Guide [10].

4. Simulation results

4.1. Methane flame

Simulations results for the methane flame are represented in figure 2 by the instantaneous resolved fields of temperature and surface incident radiation and in figure 3 by soot volume fraction. The latter is shown for two oxidation models, by Fenimore and Jones [11] and by Lee et al. [12].

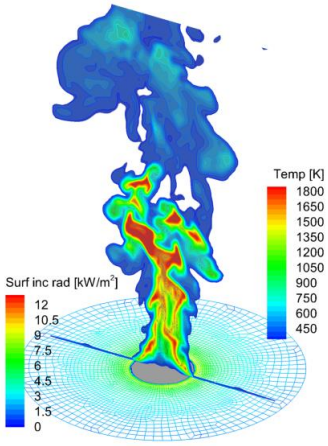

Figure 2. Instantaneous resolved temperature and incident radiation at the floor surface

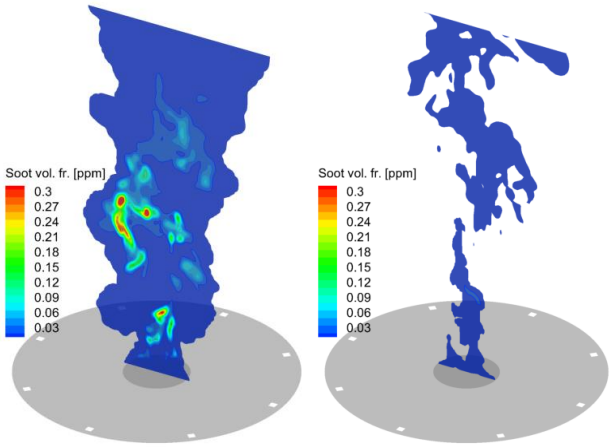

Figure 3. Instantaneous resolved soot volume fraction distributions predicted by the Moss-Brooks model: left – Fenimore-Jones oxidation; right – Lee et al. oxidation.

Simulations revealed a remarkable difference between the soot volume fraction distributions predicted with the different soot formation models available in ANSYS FLUENT. Here, we restrict discussion to considering the most comprehensive approach, the Moss-Brooks model. The simulations shown that, given the soot formation model, the predicted soot volume fraction spatial distribution and the soot yield in the overfire region is also very sensitive to the soot oxidation model (figure 3). In the methane flame, when the Fenimore-Jones oxidation model (default option in ANSYS FLUENT) is applied, the predicted soot yield, 1.5 g soot per 1 g fuel burned, appears to be much higher than the literature data (close to zero). Replacing the OH oxidation mechanism (the Fenimore-Jones model [11]) by the O_2 oxidation mechanism (oxidation model by Lee et al. [12]) results in strong reduction of the soot yield from the flame. Thus, a possible reason for the overestimated predictions of the soot yield is underestimated soot oxidation rate by the Fenimore-Jones model.

Simulations have shown (figure 4) that switching between the Fenimore and Jones' and the Lee' et al. models result in strong changes not only in the oxidation rates, but also in soot formation rates. If the OH-driven oxidation is the only mechanism taken into account in Eq. (4), then a considerable positive difference between the integral surface growth rate and the oxidation rate can be observed. Jointly with the contribution by the nucleation rate (which is rather small, note the scale for this term in figure 4, left), this difference is the indication of an appreciable amount of soot leaving the flame.

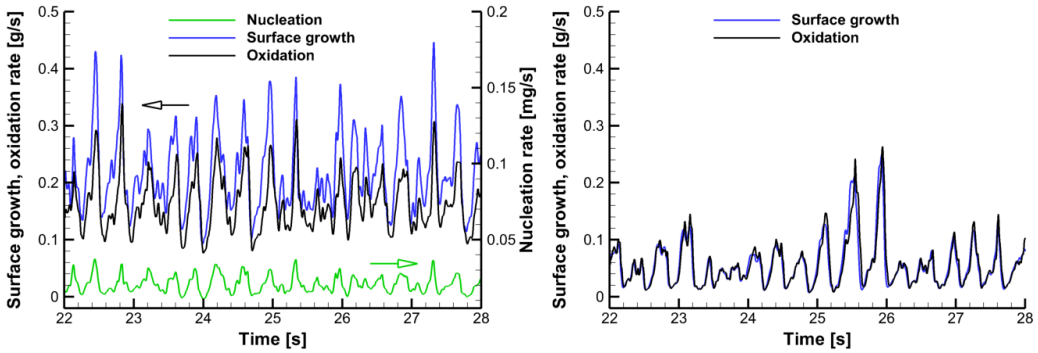

Figure 4. Total surface growth, oxidation and nucleation rates predicted with the Moss-Brooks model: left – Fenimore-Jones oxidation; right – Lee et al. oxidation.

When the alternative oxidation term is activated in Eq. (4) (oxidation by O_2), not just the oxidation rate but also surface growth rate decrease greatly (by a factor of four, approximately). Most importantly, total surface growth and oxidation rates now equilibrate each other, and the nucleation term results in a negligible soot mass production. As a result of such an equilibrium, much smaller amount of soot escapes to the overfire region. It can therefore be concluded that the Lee et al. term in Eq. (4), which is responsible for oxidation by molecular oxygen, plays a stronger role than that corresponding to OH-driven soot oxidation.

In figure 5, predicted radiative fluxes incident to the horizontal (floor level) and vertical (0.732 m away from the flame axis) surfaces are compared with those measured in [2]. Given the magnitude of turbulent fluctuations, the overall agreement is quite good.

The effect of soot model was also analyzed by comparing the predicted values of integral radiative quantities, radiative fraction and flame absorptivity. When the Moss-Brooks soot formation model is applied with the Fenimore-Jones or Lee et al. oxidation models, maximum instantaneous soot volume fractions fluctuate strongly around the mean values of about 1 ppm and 0.4 ppm, respectively. Reduced soot volume fraction results in lower radiative losses and flame absorptivity and, therefore, in higher maximum resolved temperatures. Indeed, the time-averaged values of the latter are found to be 2164 K (Fenimore-Jones) and 2204 K (Lee et al.). Instantaneous values of the radiative fraction exhibit strong transient fluctuations, and the peak values could be twice as higher than the time-

averaged values. The radiative fraction of 0.18 predicted by the Moss-Brooks soot, Lee et al. oxidation models appear to be very close to the case when no soot formation was accounted for. It can be attributed to the fact that soot forms in the cold fuel-rich region, while in the near-stoichiometric peak temperature zone soot is already oxidized. It also shows that radiation emission in this flame is dominated by the gaseous products rather than by soot. The methane flame considered in this work remains to be optically thin since only 13 to 15% (on average) of the radiative energy emission is reabsorbed by the flame.

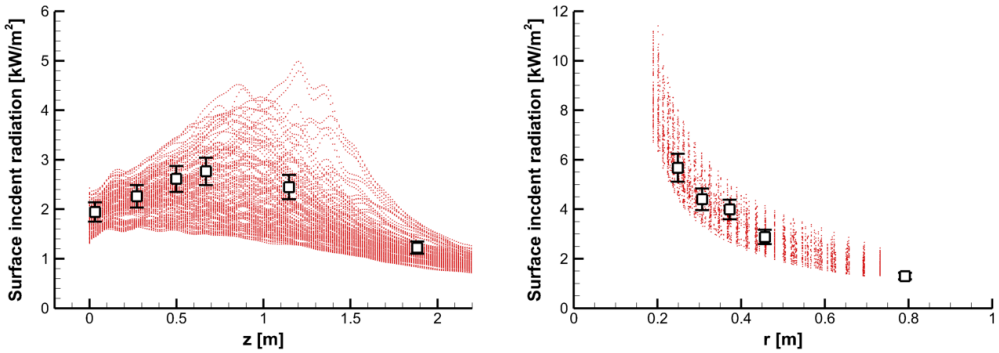

Figure 5. Predicted and measured distributions of surface incident radiative flux along vertical (left) and horizontal (right) surfaces. Dots – ANSYS FLUENT simulations with the Moss-Brooks soot model (Lee et al. oxidation), symbols with error bars – measurements [2].

4.2. Heptane flame

Instantaneous resolved fields of temperature, soot volume fraction, radiation emission and absorption are illustrated in figure 6. Burning of heptane yields a much greater amount of soot than that of methane. This difference can be accounted for by modifying the precursor mole fraction, X_{prec}, in the soot formation (nucleation and surface growth terms) in equations (3) and (4). In this study, we retain the same dependence of the precursor mole fraction on the mixture fraction, as that used by default in ANSYS FLUENT for methane, and increase the model constants, C_{α} and C_{γ}. More specifically, we increase both constant by the same factor, which is optimized to simultaneously replicate experimental data for the flame radiative impact and the soot yield.

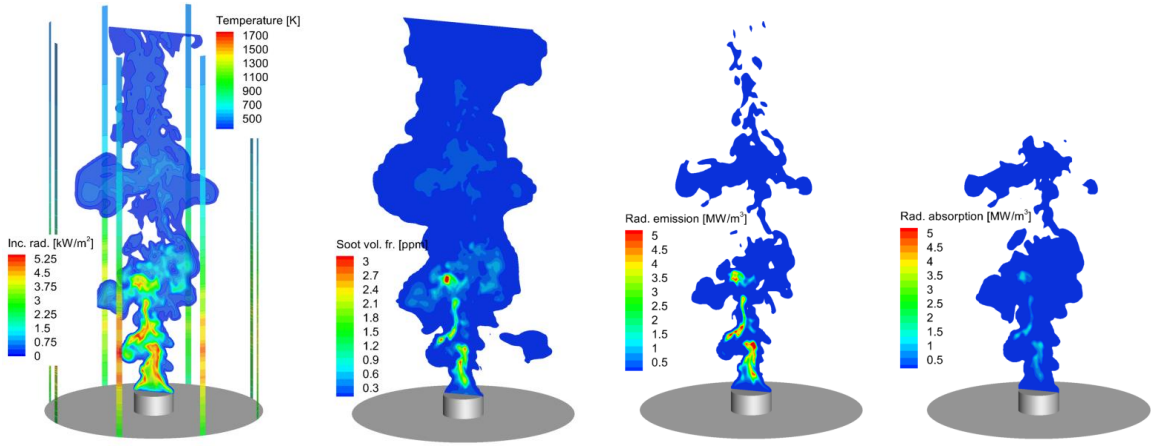

Figure 6. Instantaneous resolved distributions in the axial plane of 116 kW heptane flame above 0.3 m diameter burner, left to right: temperature (surface incident radiation along the vertical strips is also shown), soot volume fraction, radiation emission, radiation absorption.

The simulation results were found to be very sensitive to the abovementioned factor. Indeed, the excessively high value causes overestimated soot nucleation and surface growth rates, soot volume fraction and radiation emission. As a result, flame temperature is reduced, which leads to a further reduction of the soot oxidation rate. Alternatively, if the factor is too low, both the soot yield and the radiative fluxes are underestimated. Current simulations show that increasing the default values of C_α and C_γ by a factor of three provides most realistic simulation results.

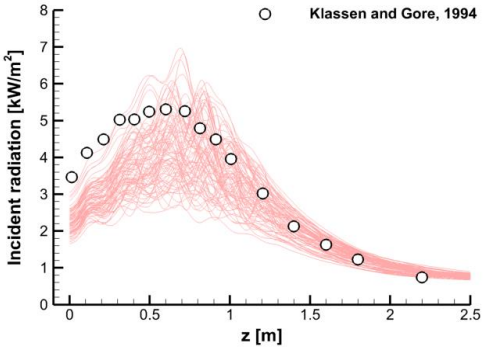

Figure 7. Predicted and measured distributions of surface incident radiative flux along vertical surfaces. Lines – ANSYS FLUENT simulations with the modified Moss-Brooks soot model (Lee et al. oxidation), symbols – measurements [3].

Predicted vertical distributions of radiative fluxes at a distance 0.825 away from the flame axis to the measurements are shown in figure 7, and predicted transient variation of the radiative fraction is given in figure 8, left. Comparison of the former with the measurements [3] indicate that predicted radiation emission is somewhat underestimated, albeit, on average, the soot yield is higher than the value of 0.04 reported, for example, in [13]. A possible reason of underestimated radiation emission is limited spatial resolution and neglecting subgrid temperature fluctuations, due to which $\tilde{\kappa}\tilde{T}^4 < \kappa T^4$. Note, that the approximate relation, $\kappa T^4 \approx \tilde{\kappa}\tilde{T}^4\left(1+const\,T'^2/\tilde{T}^2\right)$ proposed in [14] could be applied to allow for the TRI effects.

Further analysis shows that, dissimilar to the methane combustion, radiation emission in the heptane-fuelled flame is dominated by soot. As such, reliable predicting both soot formation and soot oxidation becomes particularly important, and these submodels should be further examined when applied to the buoyant flames. Nevertheless, the above simulation results indicate potential possibility of predicting frame radiative impact based on the first principles, with no pre-assumed radiative fraction.

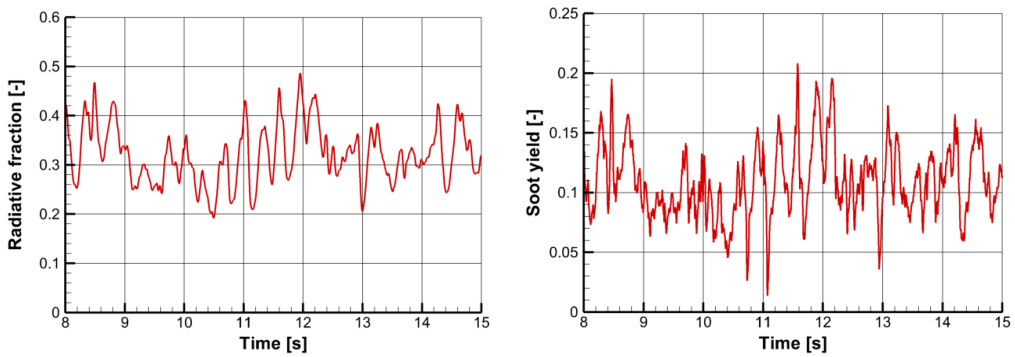

Figure 8. Predicted radiative fraction (left) and soot yield (g soot per g fuel, right) with the modified Moss-Brooks soot model (Lee et al. oxidation).

5. Conclusions

By means of the large eddy simulations we evaluated soot formation and oxidation, as well as flame radiation, in two buoyant turbulent diffusion flames fuelled by methane and heptane. These flames exhibit very different relative contributions of gas and soot in radiation emission, which was evaluated in this work based on the instantaneous resolved temperatures and product concentrations. As such, we followed a more fundamental approach than that used in many practical fire simulations, in which the local emission term is recalibrated to provide the total radiated energy to be equal to a pre-assumed fraction, f_r, of the total heat release rate in the flame.

Three soot models available in ANSYS FLUENT (the one-step model by Khan and Greeves, the two-step model by Tesner et al., and the Moss-Brookes model) produced very different results, which were strongly affected both by the soot formation and soot oxidation submodels. For the methane flame, it has been demonstrated that the both soot formation and soot oxidation components are equally important. When combined with the Moss-Brooks model, the default option of Fenimore-Jones oxidation results in predicting a considerable soot yield being in contrast with the experimental observations for overventilated methane flames. Among the soot source terms, the Lee et al. oxidation term (oxidation by molecular oxygen) dominates over the Fenimore-Jones oxidation term (oxidation by hydroxyl radical) and results in better agreement between the predicted and measured soot yields for the methane flame considered in this work.

For the simulated methane fire, soot contribution into predicted flame radiation was found to be below 25% of the overall radiative fraction, which corresponds to 5% of total heat release rate. Predicted radiative heat fluxes were found in best agreement with the measurement data for both horizontal and vertical exposed surfaces, when the Moss-Brooks soot formation model was applied jointly with the Lee at al. oxidation model.

For the heptane fire, the Moss-Brooks soot formation model has been recalibrated, and a dominating contribution of soot radiation was demonstrated.

6. References

[1] Crosland B M, Thomson K A and Johnson M R 2015 *Proc. Combust. Inst.* **35** 1851
[2] Hostikka S, McGrattan K B and Hamins A 2003 Numerical modeling of pool fires using LES and finite volume method for radiation *Fire safety science – Proc. 7th Int. Symp.* (IAFSS) pp 383-394
[3] Klassen M and Gore G P 1994 Structure and radiation properties of pool fires *NIST Report NIST-GCR-94-651*
[4] Snegirev A Yu and Tsoy A S 2015 *Proc. Combust. Inst.* **35** 2519
[5] Snegirev A Yu 2015 *Combust. Flame* **162** 3622
[6] Heskestad G 2002 Fire Plumes, Flame Height, and Air Entrainment *SFPE Handbook of Fire* Protection Engineering (Quincy MA: NFPA) pp 2-1–2-17
[7] Smith T F, Shen Z F and Friedman J N 1982 *J Heat Transfer* **104** 602
[8] Taylor P B and Foster P J 1974 *Int. J. Heat Transfer* **18** 1331
[9] Brookes S J and Moss J B *Combust. Flame* **116** 486
[10] ANSYS FLUENT Theory Guide, Release 15, ANSYS Inc., 2013
[11] Fenimore C P and Jones G W 1967 *J. Phys. Chem.* **71** 593
[12] Lee K B, Thring M W and Beer J M 1962 *Combust. Flame* **6** 137
[13] Ditch B D, de Ris J L, Blanchat T K, Chaos M, Bill R G Jr and Dorofeev S B 2013 *Combust. Flame* **160** 2964
[14] Snegirev A Yu 2004 *Combust. Flame* **136** 51